Sensors and Materials, Vol. 35, No. 7 (2023) 2619–2635
MYU Tokyo

S & M 3344

Fast Maximum Power Tracking for Photovoltaic Module Array Using Only Voltage and Current Sensors

Thi Bao Ngoc Nguyen and Kuei-Hsiang Chao*

Department of Electrical Engineering, National Chin-Yi University of Technology
No. 57, Sec. 2, Zhongshan Rd., Taiping Dist., Taichung 41170, Taiwan

(Received January 30, 2023; accepted June 22, 2023)

Keywords: voltage and current sensors, photovoltaic module array, maximum power point tracking, improved power feedback method, power-voltage characteristic curve, tracking speed response, steady-state performance

In this paper, we describe the research and development of the maximum power point tracker (MPPT) for a photovoltaic module array (PVMA) under different sunlight intensities and temperatures. In this study, an improved power feedback method (IPFM) is used to track the maximum power point (MPP) of the PVMA. Because a traditional power feedback method (PFM) is used for maximum power tracking, once the sunlight intensity and temperature change, the MPP of the PVMA changes accordingly. Nevertheless, the fixed duty cycle variation of the boost converter is used for the tracking step in the traditional PFM, so that it may take a long time to track to the MPP. For this reason, an MPPT based on the IPFM is proposed in this paper, so that its tracking step is adjusted adaptively according to the slope of the power-voltage (P–V) characteristic curve of the PVMA. Moreover, the initial voltage for starting tracking is set to 0.8-fold the MPP voltage V_{mp} of the PVMA under standard test conditions (STCs). First, a programmable DC power supply (62050H-600S) produced by Chroma ATE Inc. is used in this study to simulate the output characteristics of a 4-series and 1-parallel PVMA, and then simple voltage and current sensors are used to feed back the voltage and current of the PVMA, followed by MPP tracking by the IPFM. From the experimental results, it is proved that the proposed IPFM yields a better tracking speed response and steady-state performance than the traditional PFM under different working environments.

1. Introduction

A photovoltaic power generation system is composed of a photovoltaic module array (PVMA) and a power conditioner including a DC/AC converter, a DC/DC converter, a system controller, and a parallel protection device. In the photovoltaic power generation system, if the PVMA is connected to a load directly, the output power of the module array is determined by the load, so that the maximum output power of the PVMA is unavailable. Therefore, the maximum power point tracker (MPPT) needs to be connected between the module array and the load, so that it

*Corresponding author: e-mail: chaokh@ncut.edu.tw
https://doi.org/10.18494/SAM4342

ISSN 0914-4935

can achieve the optimal power generation efficiency under any sunlight intensity. At present, the most commonly used maximum power tracking methods for the PVMA among commercially available power conditioners include the constant voltage method (CVM),[1–3] power feedback method (PFM),[4,5] incremental conductance (INC) method,[6–8] and perturb and observe (P&O) method.[9–11] Among these methods, the principle of the CVM is the simplest; it regulates the output voltage of the PVMA to the maximum power point (MPP) voltage V_{mp} under the standard test condition (STC) for any sunlight intensity. However, as the sunlight intensity changes, the voltage of the MPP changes accordingly. Although the voltages of MPPs are still almost distributed on the same vertical line, the real MPP cannot be tracked when the sunlight intensity is weak. For the working principle of the PFM, the voltage and current of the PVMA are fed back through voltage and current sensors to calculate current output power, followed by calculating the slope dP/dV based on the change rates of the output power and output voltage, by which the tracking direction is determined. This method is advantageous because of its relatively simple and easy implementation, capability of reducing power loss, and in turn, improvement of the overall power generation efficiency. However, the tracking speed response and steady-state performance are not good owing to the fixed values used for the tracking steps.

As for the principle of the P&O method, the output voltage variation of the PVMA is controlled with a fixed duty cycle variation, followed by calculating the power by feeding back the voltage and current of the PVMA, and then the current output power is compared with the previous output power to determine the next perturbation direction. If the output power increases after the perturbation, the next perturbation continues to control the output voltage of the PVMA in the same direction; in contrast, if the output power of the PVMA decreases after the perturbation, it is controlled in the opposite direction next time. With respect to the MPP tracking performed by the P&O method, the implementation is easy, but the back and forth oscillation occurs in the vicinity of the MPP, resulting in power loss. Therefore, the selection of the perturbation step size becomes very important. Although a smaller step size can reduce the oscillation in the vicinity of the MPP, it reduces the tracking speed. Hence, the magnitude of the perturbation step size is a key factor for the tracking performance of the P&O method.[12] In addition, as the external environmental conditions change more rapidly, this method may not be able to adjust the tracking direction in time, resulting in incorrect determinations.

The control concept of the INC method is similar to that of the PFM, both of which use a zero slope ($dP/dV = 0$) at the MPP on the curve of the output power and voltage of the PVMA as a determination condition. Thus, $dI/dV = -I/V$ is used to make a logical determination for the INC method after derivation, where V and I are the output voltage and output current of the PVMA, and dI/dV and I/V are the dynamic conductance and static conductance, respectively. However, owing to the complexity of the tracking process for the INC method, more parameters are required, resulting in a lower tracking speed. Moreover, owing to the impact of the sensing elements on the measurement error, the real MPP cannot be tracked. Moreover, because the differential term dI/dV is used as a determination condition, it is susceptible to noise interference.

To improve the shortcomings of various traditional MPP tracking methods mentioned, in this paper, an improved power feedback method (IPFM) is proposed to track the MPP of the PVMA. First, the characteristic curves of the PVMA are discussed, and then the theory of the IPFM is

described, by which the MPP tracking test for the PVMA is carried out. Finally, the experimental results prove that the proposed IPFM improves the shortcomings of the traditional MPP tracking methods.

2. Proposed MPP Tracking Method

The variations of output power and voltage of the PVMA are used in the PFM as the determination condition. This tracking method can improve the shortcomings of the CVM, which cannot track to the real MPP as the sunlight intensity changes, while reducing the complexity and instability from the INC method and the P&O method.

2.1 Traditional PFM

The PFM calculates the current power through the feedback voltage and current, followed by using the dP/dV slope value as the determination condition for tracking the MPP. As shown in Fig. 1, if dP/dV > 0, this indicates that the current operating point is on the left side of the MPP, so that the voltage of the PVMA has to be increased; that is, the duty cycle of the converter is reduced, such that the operating point moves toward the right side of the MPP. In contrast, if dP/dV < 0, this indicates that the current operating point is on the right side of the MPP, so that the voltage of the PVMA has to be reduced in the next step; that is, the duty cycle of the converter is increased, such that the operating point moves toward the MPP on the left side until the slope of the power-voltage (P–V) characteristic curve dP/dV = 0, which indicates that the MPP has been tracked. The control flow chart for the MPP tracking is shown in Fig. 2. When the slope approaches zero, this indicates that the output power has reached the maximum value. Although

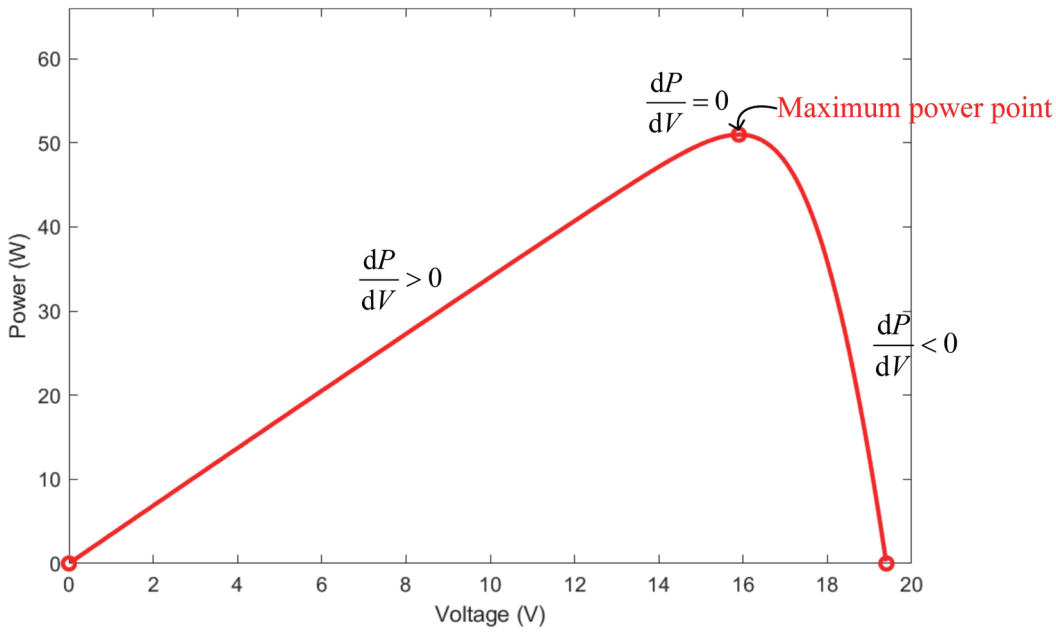

Fig. 1. (Color online) Working characteristic curve of PFM.

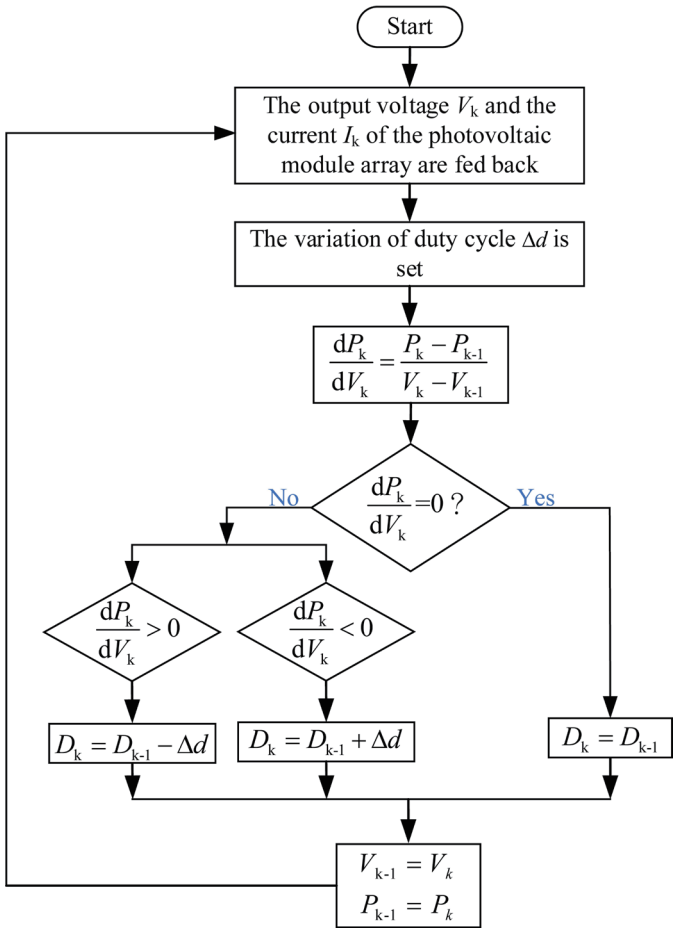

Fig. 2. (Color online) Flow chart for MPP tracking of traditional PFM.

this probability is very small, the overall efficiency is better than that of the CVM because the PFM can track to the vicinity of the MPP under different sunlight intensities, which, however, also induces power loss.

2.2 IPFM with fixed initial tracking voltage

From Fig. 3, although the *P*–*V* characteristic curves of PVMAs vary under different sunlight intensities, the MPP voltages of various curves differ insignificantly. Therefore, to improve the tracking speed of the PFM, a fixed voltage is used as the initial tracking voltage to improve the traditional PFM in this study. That is, the initial tracking voltage V_{begin} is set to be 0.8-fold the MPP voltage V_{mp} under STCs (i.e., $V_{begin} = 0.8V_{mp}$), so that each tracking begins from the voltage of V_{begin}. Therefore, even though the sunlight intensity changes, the MPP can be tracked quickly at that time with a fixed initial tracking voltage of the IPFM.

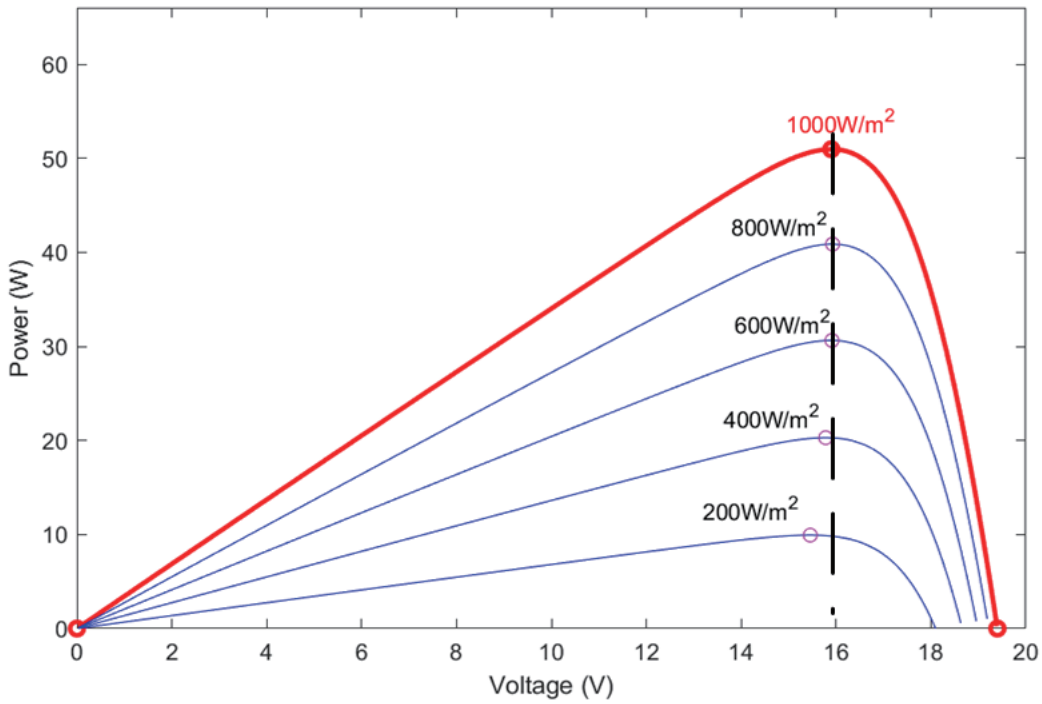

Fig. 3. (Color online) Corresponding voltages of MPPs under different sunlight intensities.

2.3 IPFM with fixed initial tracking voltage and adjusted tracking step size

Although the PFM with a fixed initial tracking voltage has a better tracking speed, the tracking speed of the system is affected if the step size is set too small because the same variation of the duty cycle is still used as the tracking step size. Nevertheless, although the speed can be increased if the setting is too large, there is a large magnitude of back and forth oscillation when tracking to the vicinity of the MPP, resulting in power loss. To avoid these problems without affecting the tracking speed, in addition to improving the PFM with a fixed initial tracking voltage, the variation of the duty cycle is adjusted automatically according to the variation range for the slope of the *P–V* characteristic curve, so that the operating point has the variation of the duty cycle decreased gradually as it gets closer to the MPP. Similarly, as the operating point gets farther away from the MPP, the variation of the duty cycle is increased, and the step size of tracking is increased. As such, the tracking speed can be increased at the same time, and the magnitude of back and forth oscillation in the vicinity of the MPP can be reduced. Moreover, when the sunlight intensity suffers from an abrupt change, the variation of the duty cycle can also be adjusted in time.

Figure 4 shows the relationship diagram of the slope interval division for which the tracking step size (that is, the variation of the duty cycle) is adjusted automatically by the IPFM according to the slope of the *P–V* characteristic curve in Table 1, wherein m is the slope of the *P–V* characteristic curve and is defined as dP/dV. From Fig. 4, the following situations can be observed.

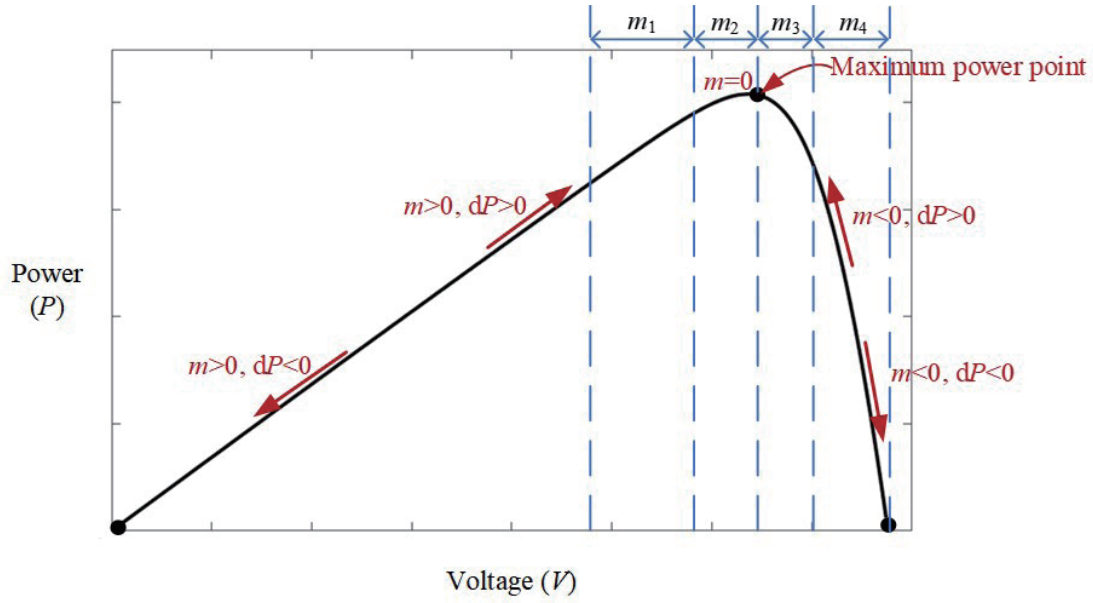

Fig. 4. (Color online) The slope interval division relationship for the variation of the duty cycle is adjusted automatically according to the slope of the P–V characteristic curve for the IPFM.

Table 1
Adjustment relationship between the slope interval of the P–V characteristic curve and the variation of the duty cycle for the converter.

Slope interval of P–V characteristic curve	Variation of duty cycle (Δd)
Interval m_1: $1.5 \geq m \geq 1$	0.005
Interval m_2: $1 > m \geq 0$	0.0005
Interval m_3: $0 > m \geq -1$	0.0004
Interval m_4: $m < -1$	0.004

(1) When the slope m is less than zero, this indicates that the system has tracked to the right side of the MPP, and the tracking is oriented to the left side of the MPP.
(2) When the slope m is larger than zero, this indicates that the system has tracked to the left side of the MPP, and the tracking is oriented to the right side of the MPP.
(3) When the slope m is equal to zero, this indicates that the system has tracked to the MPP. Moreover, the definitions for the slope m and the power variation dP are as follows:

$$m = \frac{\mathrm{d}P}{\mathrm{d}V} = \frac{P_k - P_{k-1}}{V_k - V_{k-1}}, \tag{1}$$

$$\mathrm{d}P = P_k - P_{k-1}. \tag{2}$$

Here, P_k and V_k are the power and voltage values of the current operating point, and P_{k-1} and V_{k-1} are the power and voltage values of the previous operating point, respectively.

3. Characteristic Curves of the Adopted PVMA

Since the output characteristic curve of the PVMA is nonlinear, and the output power is related to the sunlight intensity and ambient temperature, the *P–V* characteristic curve and current-voltage (*I–V*) characteristic curve at the same ambient temperature change apparently with the change in the sunlight intensity. The voltage and current of the MPP of the adopted photovoltaic module under the sunlight intensities of 1000 and 500 W/m^2 at the temperature of 25 °C are listed in Table 2.[13,14]

In this paper, the Kyocera KC50 modules[15] are connected into a 4-series and 1-parallel 202.6 W PVMA and, under sunlight intensities of 1000 and 500 W/m^2, the proposed modified PFM is used for the maximum power tracking. The output *I–V* and *P–V* characteristic curves of the PVMA are shown in Figs. 5 and 6, respectively. From the figures, under a sunlight intensity of 1000 W/m^2 and temperature of 25 °C, the MPP of the PVMA is 202.6 W, and at the same temperature, when the sunlight intensity drops to 500 W/m^2, its maximum output power is reduced to 101.8 W.

4. Converter Design for Maximum Power Tracking Control

Figure 7 shows an architecture for realizing the application of the proposed modified PFM to a PVMA for maximum power tracking. The architecture is mainly for a MPPT composed of a boost converter and an IPFM, which uses a boost converter[16,17] to modulate the output voltage

Table 2
Output of photovoltaic module at 25 °C under different sunlight intensities.

Sunlight intensity	1000 W/m^2	500 W/m^2
Voltage of MPP (V)	15.9	14.3
Current of MPP (A)	3.205	1.781
Maximum output power (W)	50.95	25.47

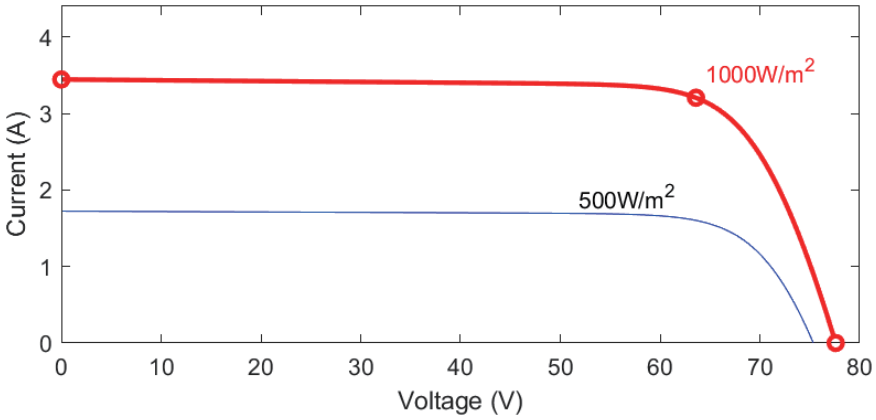

Fig. 5. (Color online) Output *I–V* characteristic curves of 4-series and 1-parallel PVMA under sunlight intensities of 1000 and 500 W/m^2 and temperature of 25 °C.

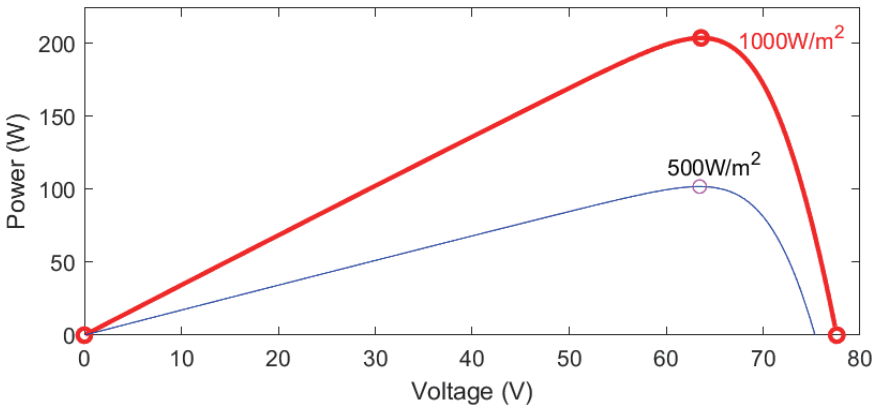

Fig. 6. (Color online) Output *P*–*V* characteristic curves of 4-series and 1-parallel PVMA under sunlight intensities of 1000 and 500 W/m^2 and temperature of 25 °C.

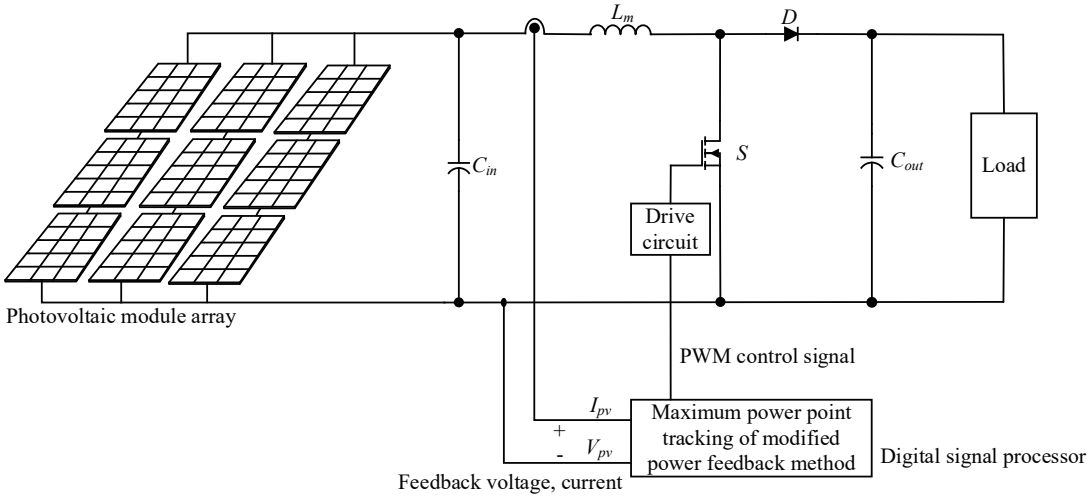

Fig. 7. Architecture of maximum power tracker for an IPFM.

of the PVMA, followed by feeding back the voltage and current signals of the PVMA by a differential amplifier, and then sending the signals to a digital signal processor[18] to calculate the duty cycle required by the converter in the next step for MPP tracking.

Figure 8(a) shows the circuit architecture of a boost converter.[19] Its components include a fast diode, an energy storage inductor, a filter capacitor, and a power switch.

Before analyzing the circuit, the following are assumed:

(1) The circuit is operable in a steady state.

(2) The switching cycle is defined as T, the on-time of switch is defined as DT, and the cut-off time is defined as $(1 - D)T$, where D is the duty cycle ($D \triangleq t_{on} / T$), and t_{on} is the on-time of switch in one cycle.

(3) The inductor has a current that is continuous and in the same direction, as well as always positive.

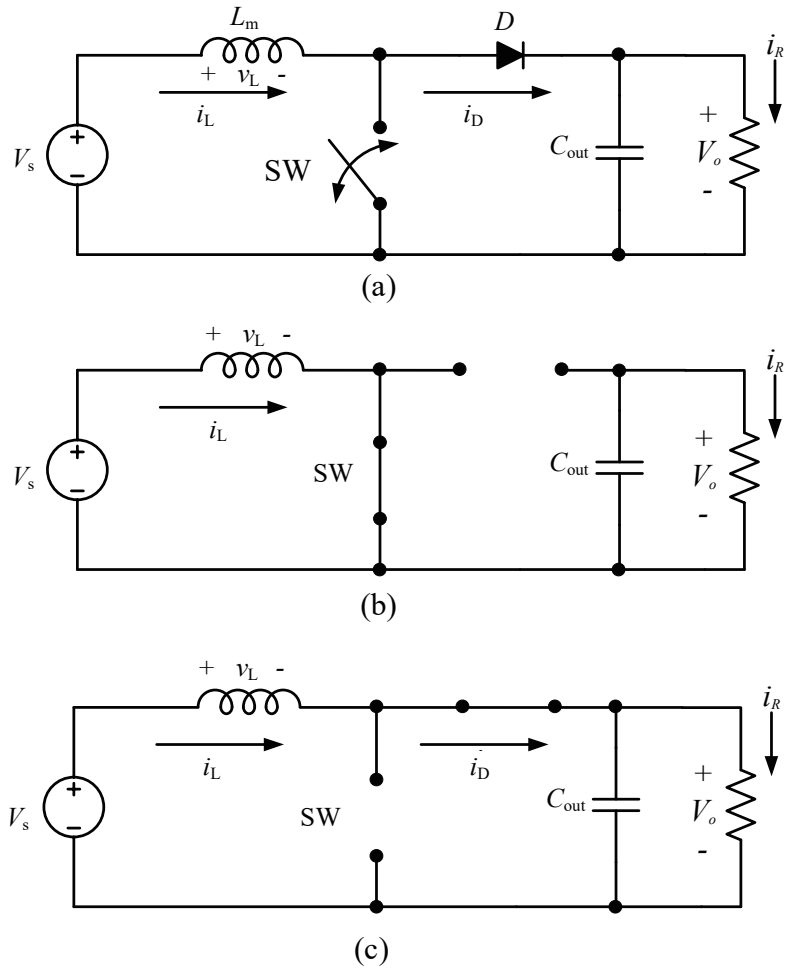

Fig. 8. Boost converter: (a) architecture of main circuit, (b) equivalent circuit when the switch SW is turned on, and (c) equivalent circuit when the switch SW is turned off.

(4) The capacitance value is extremely large, so that the output voltage V_o is constant.
(5) The circuit components are all ideal components.

When the switch SW is turned on, its equivalent circuit is as shown in Fig. 8(b). At that moment, the diode is turned off due to reverse bias. According to Kirchhoff's voltage law, we can obtain

$$V_s = L\frac{\mathrm{d}i_L}{\mathrm{d}t} \text{ or } \frac{\mathrm{d}i_L}{\mathrm{d}t} = \frac{V_s}{L}. \tag{3}$$

At that moment, the variation of current for the inductor is

$$\frac{\Delta i_L}{\Delta t} = \frac{\Delta i_L}{DT} = \frac{V_s}{L}. \tag{4}$$

From Eq. (4), the increased amount of the inductor current when the switch is turned on is

$$\left(\Delta i_L\right)_{closed} = \frac{V_s DT}{L}. \tag{5}$$

When the switch SW is cut off, the equivalent circuit of the boost converter is as shown in Fig. 8(c). At that moment, the diode is forward biased and turned on, so its circuit equation is

$$v_L = V_s - V_o = L\frac{\mathrm{d}i_L}{\mathrm{d}t}. \tag{6}$$

At that moment, the rate of change of the inductor current is negative, which is expressed as

$$\frac{\Delta i_L}{\Delta t} = \frac{\Delta i_L}{(1-D)T} = \frac{V_s - V_o}{L}. \tag{7}$$

From Eq. (7), the decreased amount of current during the cut-off of the switch could be

$$\left(\Delta i_L\right)_{open} = \frac{\left(V_s - V_o\right)(1-D)T}{L}. \tag{8}$$

According to the inductor volt-second balance principle, Eq. (9) has to be satisfied as

$$\left(\Delta i_L\right)_{closed} + \left(\Delta i_L\right)_{open} = 0. \tag{9}$$

Therefore, it can be deduced from Eqs. (5) and (8) that

$$V_o = \frac{V_s}{1-D}, \tag{10}$$

where V_o is the output voltage, V_s is the input voltage, and D is the duty cycle.

Since the duty cycle D is a value between 0 and 1, the output voltage is always greater than or equal to the input voltage, so that the converter is a boost converter.

In this paper, the switching frequency of the switch is selected as 25 kHz. After calculation, the inductance value, capacitance value, and specifications of relevant components for the boost converter can be obtained[19] as shown in Table 3.

5. Experimental Results and Discussion

A programmable DC power supply (62050H-600S)[20] produced by Chroma ATE Inc. was used in this study to simulate the output characteristics of a 4-series and 1-parallel PVMA,

Table 3
Component specifications for boost converter.

Components	Specifications
Filter capacitance C_{out}	470 μF, rated voltage 450 V
Energy storage inductance L_m	1.67 mH, rated current 7.4 A
Fast diode D IQVD60E60A1	Rated voltage 600 V, rated current 60 A
Power switch IREP460B	Rated voltage 500 V, rated current 20 A

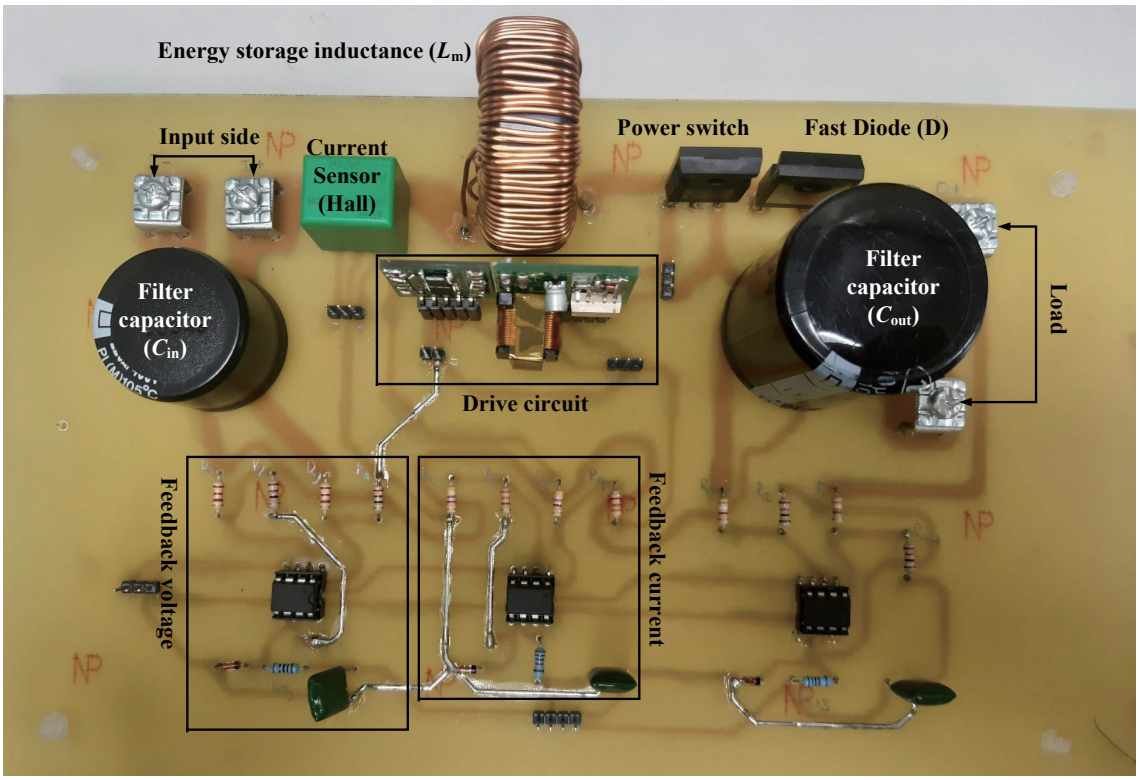

Fig. 9. (Color online) Appearance diagram of a physical circuit for tracking the MPP of the PVMA.

followed by tracking its MPP with the traditional and modified PFMs. Figure 9 shows an appearance diagram of a physical circuit used for tracking of the MPP.

First, the MPP was tracked under the sunlight intensity of 1000 W/m^2. At that moment, the MPP voltage V_{mp} of the module was 63.6 V, and the MPP current I_{mp} was 3.205 A, so that the maximum power P_{mp} of 203.8 W was obtained from the multiplication of V_{mp} and I_{mp}. From Fig. 10, the tracking time required to track the MPP using the traditional PFM was 3.18 s. Figures 11 and 12 show the test results using the PFM with fixed initial tracking voltage and with fixed initial tracking voltage together with adjustment of step size via the slope of the P–V characteristic curve, respectively. From Fig. 11, the improved method with fixed initial tracking voltage was adopted, such that the time for tracking the MPP was 2.62 s. From Fig. 12, the MPP

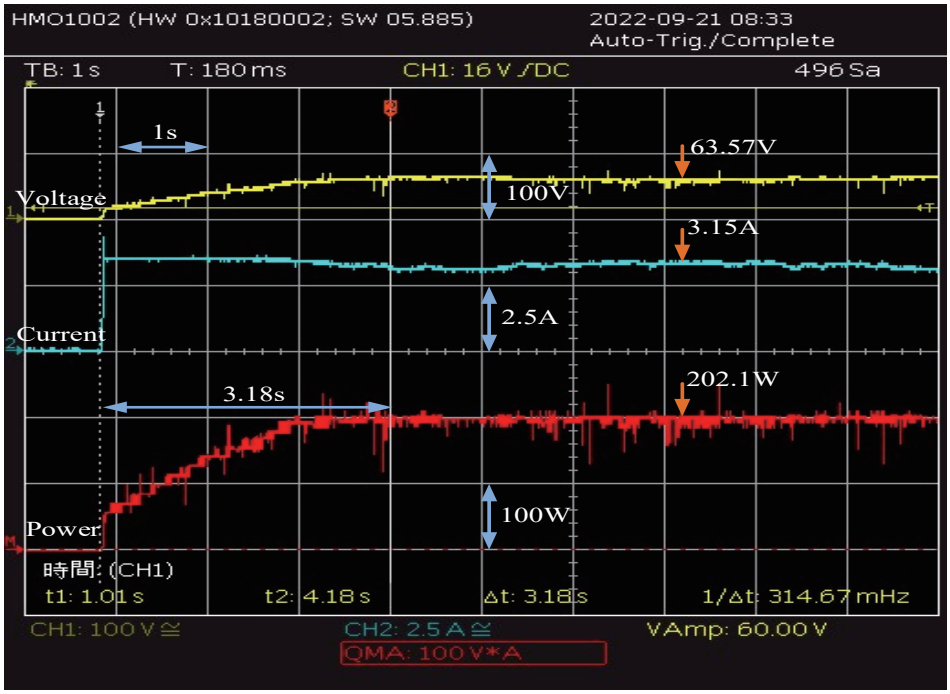

Fig. 10. (Color online) Measured waveforms from the tracking of the MPP using the traditional PFM under sunlight of 1000 W/m^2.

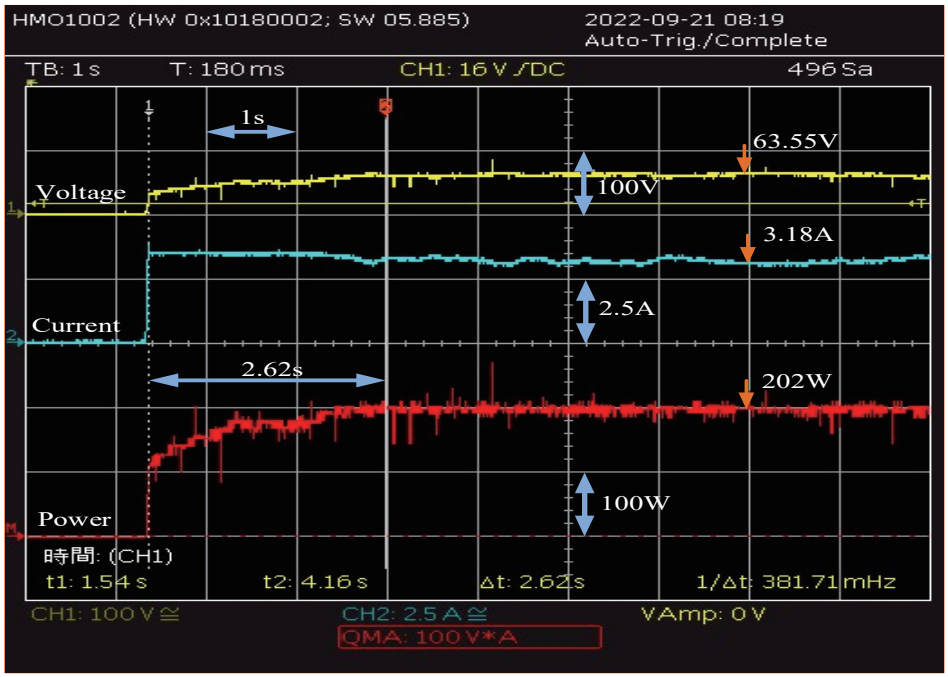

Fig. 11. (Color online) Measured waveforms from the tracking of the MPP using the PFM with fixed initial tracking voltage under sunlight of 1000 W/m^2.

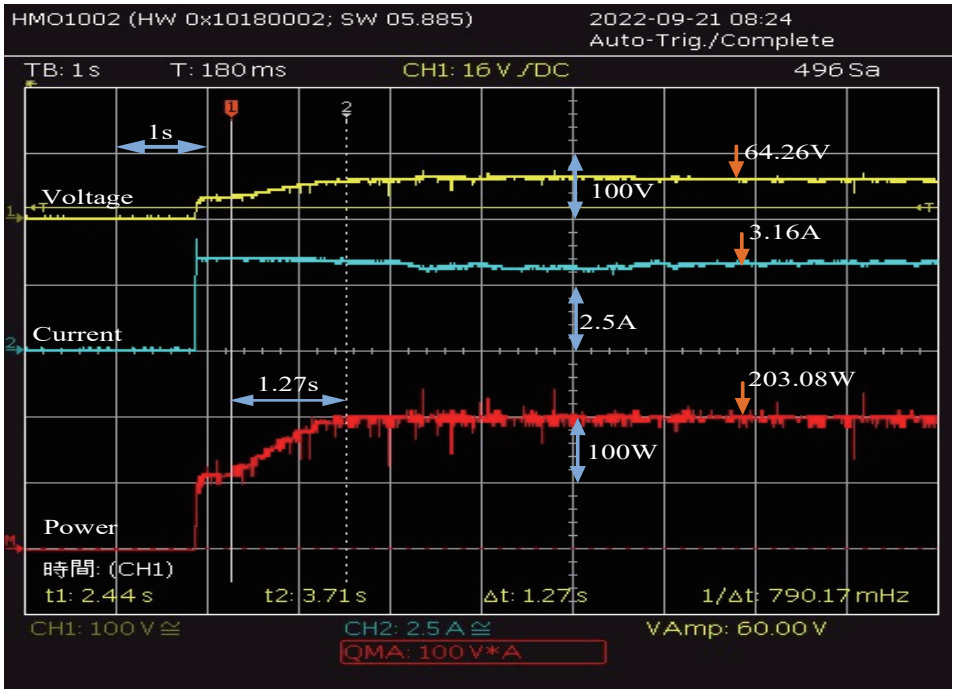

Fig. 12. (Color online) Measured waveforms from the tracking of the MPP using the PFM with fixed initial tracking voltage together with adjustment of step size via the slope of the *P–V* characteristic curve under sunlight of 1000 W/m^2.

tracking method using the fixed initial tracking voltage together with the adjustment of the step size via the slope of the *P–V* characteristic curve was adopted, such that the time required to track to the MPP was only 1.27 s. This is the fastest among the three methods.

The MPP was tracked under a sunlight intensity of 500 W/m^2. At that moment, the MPP voltage V_{mp} of the 4-series and 1-parallel module array was 57.2 V and the MPP current I_{mp} was 1.781 A, so that the maximum power P_{mp} of 101.9 W was obtained from the multiplication of V_{mp} and I_{mp}. From Fig. 13, the time required to track the MPP using the traditional PFM was 4.78 s. From Fig. 14, the time required for tracking the MPP using the IPFM with fixed initial tracking voltage was shortened to 3.93 s. As for Fig. 15, the MPP was tracked by using the IPFM with fixed initial tracking voltage together with the adjustment of the step size via the slope of the *P–V* characteristic curve, by which the time required to track the MPP was only 2.7 s. This method achieved the shortest MPP tracking among the three methods.

From the experimental results, it was proved that the IPFM developed in this study yields a better tracking speed response and steady-state performance than the traditional PFM under different working environments. The time taken to track to the MPP under different conditions for the three different tracking methods is summarized in Table 4 for comparison. From Table 4, it is clear that the PFM with fixed initial tracking voltage together with the adjustment of the step size via the slope of *P–V* characteristic curve proposed in this paper achieved the best tracking speed response under different sunlight intensities.

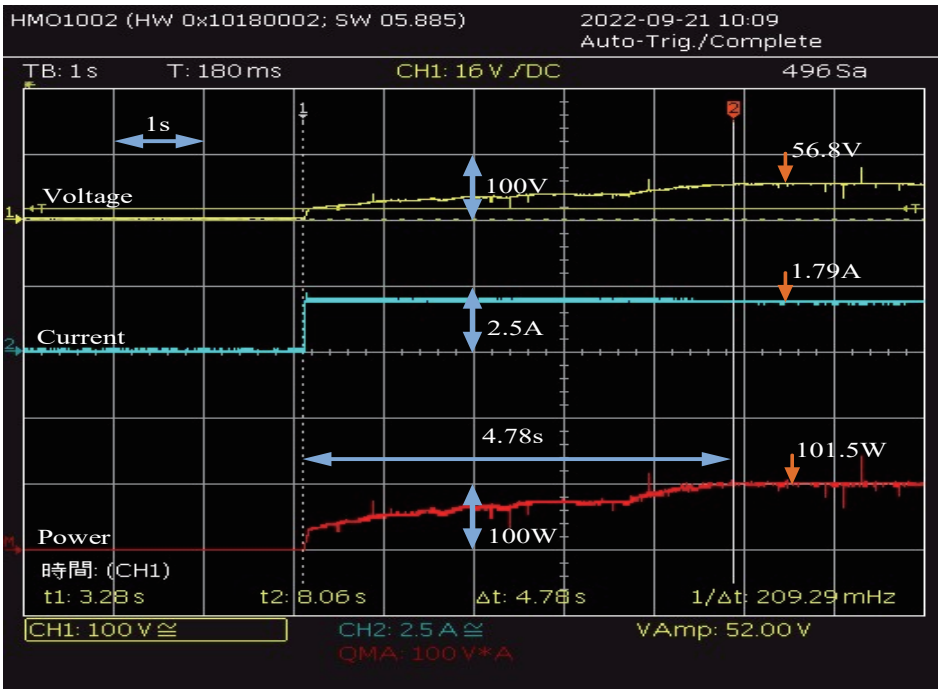

Fig. 13. (Color online) Measured waveforms from the tracking of the MPP using the traditional PFM under sunlight of 500 W/m^2.

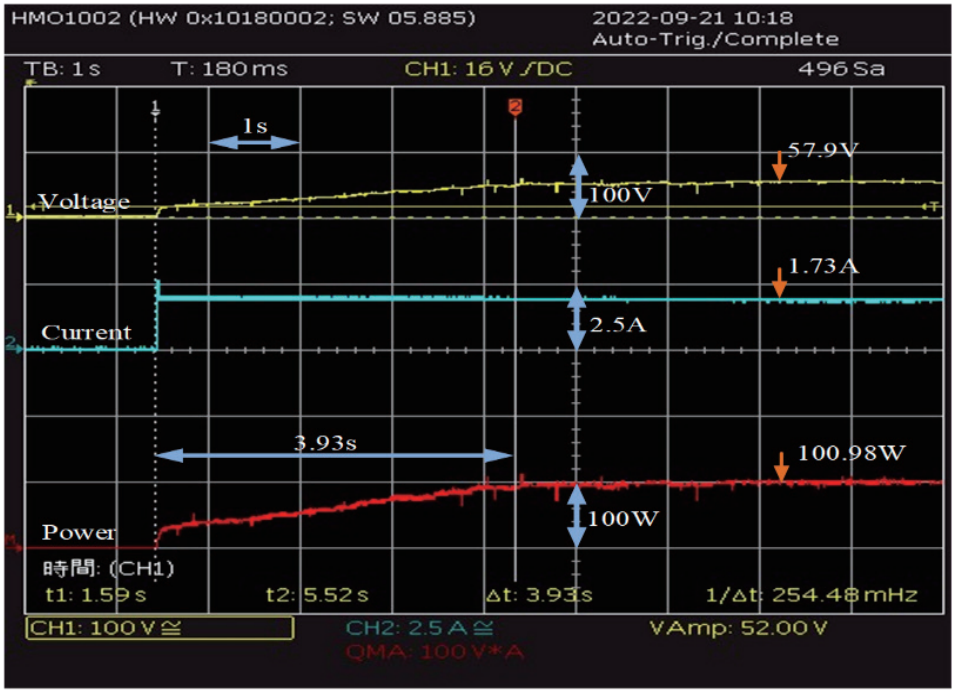

Fig. 14. (Color online) Measured waveforms from the tracking of the MPP using the PFM with fixed initial tracking voltage under sunlight of 500 W/m^2.

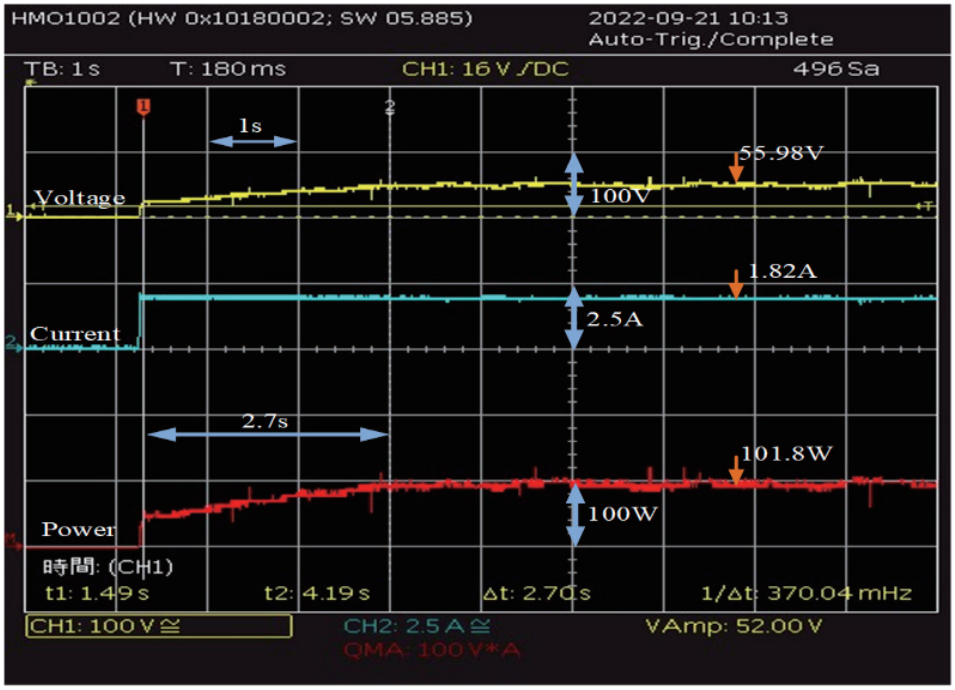

Fig. 15. (Color online) Measured waveforms from the tracking of the MPP using the PFM with fixed initial tracking voltage together with adjustment of step size via the slope of the *P–V* curve under the sunlight of 500 W/m^2.

Table 4
Comparison of the time for tracking to the MPP using the three different methods.

Tracking method	Sunlight intensity	
	1000 W/m^2	500 W/m^2
Traditional PFM (s)	3.18	4.78
PFM with fixed initial voltage (s)	2.62	3.93
PFM with fixed initial voltage together with adjustment of step size via slope of *P–V* curve (s)	1.27	2.7

6. Conclusions

The improvement of tracking performance for the MPPT based on the traditional PFM is described in this paper. By fixing the initial tracking voltage of the traditional PFM at 0.8-fold the MPP voltage under STCs, together with dividing the output *P–V* curve of the PVMA into four slope intervals, the tracking step size is adjusted and applied for tracking the MPP of the PVMA. The IPFMs proposed in this paper include the PFM with fixed initial tracking voltage and the PFM with fixed initial tracking voltage together with the adjustment of the step size via the slope of the *P–V* curve. Among them, the PFM with the fixed initial voltage together with the adjustment of the tracking step size via the slope of the *P–V* curve achieves the best tracking speed response. The proposed IPFM not only achieves a better tracking response speed than the traditional PFM, but it can also reduce power loss and improve the power generation efficiency.

From the experimental results, it is proved that when the sunlight intensity changes abruptly, all of the proposed IPFMs can track the MPP at that moment in time. Moreover, this method together with the adjustment of the tracking step size via the slope of the P–V curve can reduce the magnitude of the back and forth oscillation after the MPP is tracked, so that the power loss can be reduced and the steady-state tracking performance can be improved.

Acknowledgments

This work was supported by the Ministry of Science and Technology, Taiwan, under Grant no. MOST 110-2221-E-167-007-MY2.

References

1 M. A. S. Masoum, H. Dehbonei, and E. F. Fuchs: IEEE Trans. Energy Convers. **17** (2002) 514. https://doi.org/10.1109/TEC.2002.805205
2 G. J. Yu, Y. S. Jung, J. Y. Choi, and G. S. Kim: Solar Energy. **76** (2004) 455. https://doi.org/10.1016/j.solener.2003.08.03
3 R. Kiranmayi, K. V. K. Reddy, and M. V. Kumar: J. Eng. Applied Sci. **3** (2008) 128. https://docsdrive.com/pdfs/medwelljournals/jeasci/2008/128-133.pdf
4 E. Koutroulis, K. Kalaitzakis, and N. C. Voulgaris: IEEE Trans. Power Electron. **16** (2001) 46. https://doi.org/10.1109/63.903988
5 L. Wu, Z. Zhao, and J. Liu: IEEE Trans. Energy Convers. **22** (2007) 881. https://doi.org/10.1109/TEC.2007.895461
6 M. A. Elgendy, B. Zahawi, and D. J. Atkinson: IEEE Trans. Sustain. Energy **4** (2013) 108. https://doi.org/10.1109/TSTE.2012.2202698
7 T. T. Esram and P. L. Chapman: IEEE Trans. Energy Convers. **22** (2007) 439. https://doi.org/10.1109/TEC.2006.874230
8 T. Y. Kim, H. G. Ahn, S. K. Park, and Y. K. Lee: Proc. IEEE Int. Symp. Ind. Electron. (2001) 1011–1014. https://doi.org/10.1109/ISIE.2001.931613
9 N. Fermia, G. Lisi, G. Petrone, G. Spagnuolo, and M. Vitelli: IEEE Trans. Ind. Electron. **55** (2008) 2610. https://doi.org/10.1109/TIE.2008.924035
10 N. Femia, G. Petrone, G. Spagnuolo, and M. Vitelli: IEEE Trans. Power Electron. **20** (2005) 963. https://doi.org/10.1109/TPEL.2005.850975
11 Abu Tariq and M. S. Jamil Asghar: Proc. 2006 IEEE Power India Conf. (2006) 1–5. https://doi.org/10.1109/POWERI.2006.1632509
12 T. S. Chien and T. C. Yu: Proc. Int. Conf. Power Electronics and Drive Systems (2009) 1339–1344. https://doi.org/10.1109/PEDS.2009.5385670
13 R. Faranda and S. Leva: J. Eng. Applied Sci. **3** (2008) 446. https://www.researchgate.net/publication/228961032
14 J. Brouwer, Y. Chen, K. Smedley, and F. Vacher: Proc. 18th Annual IEEE APEC (2003) 58–62. https://doi.org/10.1109/APEC.2003.1179176
15 Kyocera Photovoltaic Module KC50 Specifications: https://documents.unboundsolar.com/legacy/pdfs/module%20pdf%20folder/KC50.pdf (accessed December 2022).
16 N. Kasa, T. lida, and H. lwamoto: Proc. 8th Power Electron. Variable Speed Drives (2002) 130–135. https://doi.org/10.1049/cp:20000233
17 I. Glasner and J. Appelbaum: Proc. 19th Conv. Electr. Electron. Eng. in Israel (1996) 355–358. https://doi.org/10.1109/EEIS.1996.566988
18 TMS320F2809 Data Manual, Texas Instruments (2003). https://www.ti.com/lit/ds/symlink/tms320f28015.pdf?ts=1671446910629&reurl=https%253A%252F%252Fwww.bing.com%252F
19 D. W. Hart: Introduction to Power Electronics (Pearson Book Company, 2002) 2nd.
20 Chroma ATE Inc.: https://www.chromaate.com/en/product/dc_power_supply_62000h_series_203 (accessed December 2022).

About the Authors

Thi Bao Ngoc Nguyen received her B.S. degree in electrical engineering from National Chin-Yi University of Technology, Taichung, Taiwan, in 2022. She is now studying for a master's degree in National Chin-Yi University of Technology, Taichung, Taiwan. Her areas of interest are power electronics and maximum power point tracking for a photovoltaic module array.

Kuei-Hsiang Chao received his B.S. degree in electrical engineering from National Taiwan Institute of Technology, Taipei, Taiwan, in 1988, and his M.S. and Ph.D. degrees in electrical engineering from National Tsing Hua University, Hsinchu, Taiwan, in 1990 and 2000, respectively. He is presently a tenured distinguished professor at the National Chin-Yi University of Technology, Taichung, Taiwan. His areas of interest are computer-based control systems, applications of control theory, renewable energy, and power electronics. Dr. Chao is a life member of the Solar Energy and New Energy Association and a member of the IEEE.